OXFORD

# Identifying a Lung Stem Cell Subpopulation by Combining Single-Cell Morphometrics, Organoid Culture, and Transcriptomics

**Takashi Fujimura[1,2], Yasunori Enomoto[1,3], Hiroaki Katsura[1], Taisaku Ogawa[4], Saori Baba[1],**
**Akira Ogata[1], Akira Yamaoka[1], Katsuyuki Shiroguchi[4], Mitsuru Morimoto[*,1]** (ID)

[1]Laboratory for Lung Development and Regeneration, RIKEN Center for Biosystems Dynamics Research, Kobe, Japan
[2]Department of Drug Modality Development, Osaka Research Center for Drug Discovery, Otsuka Pharmaceutical Co., Ltd., Minoh, Japan
[3]Department of Regenerative and Infectious Pathology, Hamamatsu University School of Medicine, Higashi-ku, Hamamatsu, Japan
[4]Laboratory for Prediction of Cell Systems Dynamics, RIKEN Center for Biosystems Dynamics Research, Suita, Japan
*Corresponding author: Mitsuru Morimoto, Laboratory for Lung Development and Regeneration, RIKEN Center for Biosystems Dynamics Research, Kobe 650-0047, Japan. Tel: +81 78 306 3198; Email: mitsuru.morimoto@riken.jp

## Abstract

Single-cell RNA sequencing is a valuable tool for dissecting cellular heterogeneity in complex systems. However, it is still challenging to estimate the proliferation and differentiation potentials of subpopulations within dormant tissue stem cells. Here, we established a new single-cell analysis method for profiling the organoid-forming capacity and differentiation potential of tissue stem cells to disclose stem cell subpopulations by integrating single-cell morphometrics, organoid-forming assay, and RNA sequencing, a method named scMORN. To explore lung epithelial stem cells, we initially developed feeder-free culture system, which could expand all major lung stem cells, including basal, club, and alveolar type 2 (AT2) cells, and found that club cells contained a subpopulation, which showed better survival rate and high proliferation capacity and could differentiate into alveolar cells. Using the scMORN method, we discovered a club cell subpopulation named Muc5b^{+} and large club (ML-club) cells that efficiently formed organoids than other club or AT2 cells in our feeder-free organoid culture and differentiated into alveolar cells in vitro. Single-cell transcriptome profiling and immunohistochemical analysis revealed that ML-club cells localized at the intrapulmonary proximal airway and distinct from known subpopulations of club cells such as BASCs. Furthermore, we identified CD14 as a cell surface antigen of ML-club cells and showed that purified CD14^{+} club cells engrafted into injured mouse lungs had better engraftment rate and expansion than other major lung stem cells, reflecting the observations in organoid culture systems. The scMORN method could be adapted to different stem cell tissues to discover useful stem-cell subpopulations.

**Key words:** lung; adult stem cells; alveolar epithelial cells; bronchiolar epithelial cells; organoids; single cell analysis; morphometrics.

## Graphical Abstract
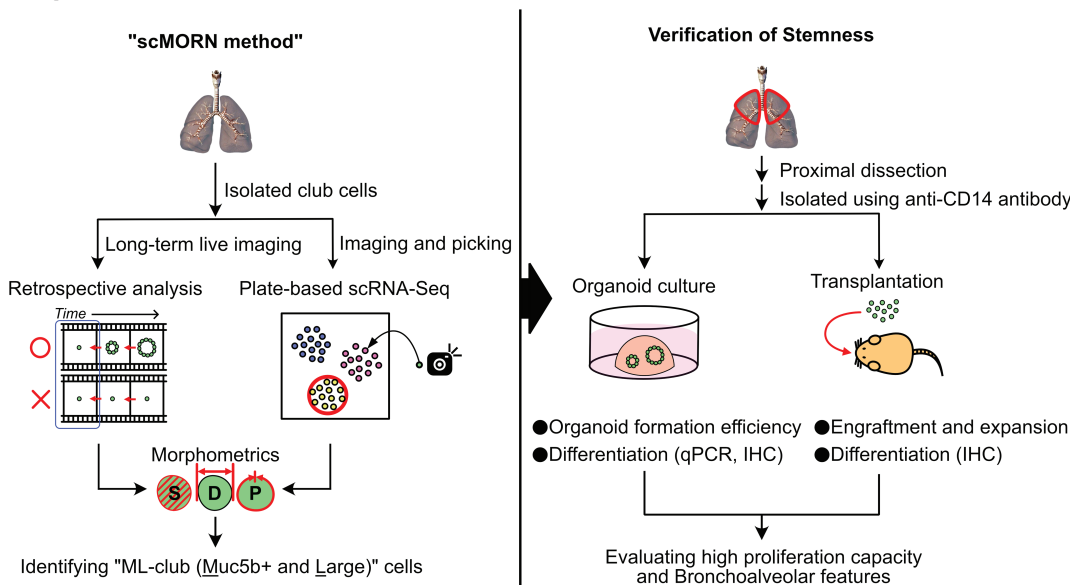
## Significance Statement

It is difficult to estimate the heterogeneous potentials of dormant adult tissue stem cells. Here, we developed a new method called single-cell morphometrics, organoid-forming assay, and RNA sequencing (scMORN) to identify stem cell subpopulations that have the capacity to form organoids and differentiate into desired cell populations. Using scMORN, we have discovered a new lung stem cell subpopulation, Muc5b-positive and large club cells (ML-club cells), which demonstrate a higher organoid formation efficiency than other stem cells and can be transplanted into an injured mouse lung.

## Introduction

Organoid culture systems with primary tissues have been used for multiple aspects, including expanding tissue stem cells as a source of cell-based therapy, assessing the differentiation capacity of stem cells, recapitulating tissue regeneration, and modeling human diseases in vitro. The organoid culture facilitates the self-organization of stem cells into a 3D tissue structure resembling partial tissue structures of real organs, including the intestine, lung, stomach, liver, and prostate.[1-6] Importantly, these organoids are clonally grown from an isolated single-stem cell, demonstrating a tremendous ability of individual stem cells to regenerate a multicellular system with a unique tissue structure. Simultaneously, the organoid-forming efficiency is generally low (eg, 6% for LGR5+ intestinal stem cells, 5% for alveolar type 2 (AT2) cells, 1.1% for LGR5+ liver stem cells, 1.4% for prostate stem cells, and 1.9% in the esophageal basal cells[6-10]), and the generated organoids are inconsistent in quality,[11] suggesting that the tissue stem cells are heterogeneous as the seeds of organoids. Dissonant organoid-formation efficiency and differentiation potential due to stem cell heterogeneity limit the contribution of organoids to basic research and translational approaches. Therefore, it is important to identify and isolate a stem-cell subpopulation with high organoid-formation capacity and able to differentiate into the cell types of interest.

The respiratory system harbors various types of epithelial tissue stem cells that maintain tissue homeostasis and repair acute damage caused by inhaled insults, such as chemical particles, viruses, and bacteria.[12-14] In the alveolar epithelium, which is located in the most distal area of the respiratory system, AT2 cells play a central role in both homeostasis and regeneration by proliferating and differentiating into alveolar type 1 (AT1) cells specialized for gas exchange.[1,15-17] Therefore, scholars have focused on the mechanisms regulating the self-renewal and differentiation of AT2 cells. These efforts have revealed heterogeneous features within the AT2 cell population.[18,19] In addition to AT2, bronchiolar club/club-like cells supply alveolar epithelial cells during regeneration following a severe injury, such as bleomycin treatment, suggesting that multiple sources of tissue stem cells provide alveolar epithelial cells.[20-22] Bronchoalveolar stem cells (BASCs), variant club/UPK3A+, and H2-K1+ cells are known as club-like cells, which are found at distal conducting airways and are capable of migration into alveoli after injury. These club-like cells then undergo transdifferentiation into AT1 and AT2 cells to cover the damaged alveolar epithelium.[21-27] These cells are a potential resource for cell-based therapy of acute alveolar injury, such as acute respiratory distress syndrome.[28]

In this study, we sought to establish an in vitro method for identifying the population of lung epithelial stem cells, which can contribute to alveolar regeneration. Single-cell RNA sequencing (scRNA-seq) is a powerful tool for profiling diverse cell populations in a high throughput manner.[29-31] However, this new technology has still difficulty in directly linking the proliferation and differentiation capacity of dormant tissue stem cell to their expression profiles. To overcome this issue, in this study, we developed a new method that can identify stem cell subpopulations having the capacity to form organoids and differentiate into the cell populations of interest by combining single-cell morphometrics, organoid-formation assay, and RNA sequencing, a method named scMORN (schematic overview in Fig. 1A). Using the scMORN method, we discovered Muc5b-positive and large club cells (ML-club cells) as a club-cell subpopulation that shows higher organoid-formation efficiency than other club or AT2 cells in our feeder-free organoid culture and can generate alveolar epithelial cells. In vivo transplantation experiments with injured lungs confirmed that ML-club cells were efficiently expanded at the damaged area more than AT2 cells and other club-cell subpopulations and differentiated into alveolar cells. We show that the scMORN method can identify a stem-cell subpopulation that generates the desired organoids.

## Materials and Methods

### Mouse Lines

The animals were housed in controlled environment rooms, and all the experimental procedures using animals were approved by the Institutional Animal Care and Use Committee of the RIKEN Kobe Branch. We handled the mice in accordance with the ethical guidelines of the institute. *SFTPC*-green fluorescent protein (*GFP*) (PMID: 18178827), *Sftpc-CreERT2* (B6.129S-*Sftpc*^tm1(cre/ERT2)Blh^/J) (PMID: 22123957, JAX Stock No: 028054), *Scgb1a1-CreER* (B6N.129S6(Cg)-*Scgb1a1*^tm1(cre/ERT)Blh^/J) (PMCID: PMC2730729, JAX Stock No: 016225), and *Rosa26-mTmG* (B6.129(Cg)-*Gt(ROSA)26Sor*^tm4(ACTB-tdTomato,-EGFP)Luo^/J) (PMID: 17868096, JAX Stock No: 007676)[20,32-34] and have been described previously. Nude mice were purchased from Nihon SLC. *Scgb1a1-CreER*; *Rosa26-mTmG* and *Sftpc-CreERT2*; *Rosa26-mTmG* mice were created by crossing *Scgb1a1-CreER*, *Sftpc-CreERT2*, and *Rosa26-mTmG*. To label *Scgb1a1-CreER* and *Sftpc-CreERT2* lineage cells, these mice were injected with tamoxifen (0.25 mg/g body weight) in peanut oil 5 times for Scgb1a1+ and 3 times for Sftpc+ cells on alternate days, and 3 weeks after the last injection; these mice were used for all experiments.

### Organoid Culture

Sorted cells were mixed in an equal volume of GFR Matrigel (#356230, Corning) and a 20-µL drop placed on the bottom of the plate, 1 drop/well in a 48-well plate or 4 drops/well in a 6-well plate. The cell number of seeded cells ranged from 150 to 5000 cells per drop. A 250-µL medium was added to the 48-well plate or 2-mL to the 6-well plate. To establish a feeder-free culture system for GFP^neg/low/hi^ cells, basic medium (DMEM/F12 containing 1× B/27, 5% FBS, 15 mM HEPES, 0.03% NaHCO₃, 250 ng/mL amphotericin B, and

1× penicillin/streptomycin) was supplemented with Y27632 (10 μM, #LCL-Y-5301-5, LC Laboratories), HGF(30 ng/mL, #2207-HG-025, R and D Systems), FGF10 (50 ng/mL, #100-26, PeproTech), KGF (50 ng/mL, #5028-KG-025, R and D Systems), NOGGIN (100 ng/mL, #250-38, PeproTech), SB431542 (10 μM, # 616461, Sigma-Aldrich), and/or CHIR99021 (3 μM, #SML1046, Sigma-Aldrich). Complete medium was basic medium supplemented with Y27632, HGF, FGF10, KGF, NOGGIN, and SB431542. The differentiation medium has the same contents as that of the basic medium. The medium was changed every 3 days. Y27632 was included in the medium for the first 3 days.

## Statistical Analysis

Statistical analyses were conducted using GraphPad Prism9 (GraphPad) or R software version 3.6.3 (https://www.r-project.org/, R Development Core Team). Two-tailed unpaired Student's *t*-test, Wilcoxson rank-sum test, one-way analysis of variance followed by Tukey's multiple comparison test, and Spearman's rank correlation coefficient were performed as shown in figure legends. $P < .05$ was considered statistically significant.

Other materials and methods are described in supplemental information.

## Results

### Club-Cell Subpopulation Transdifferentiates Into Alveolar Cells

Several groups have established mouse lung epithelial organoid culture systems, most of which require lung fibroblasts as feeder cells to support the growth of stem cells in addition to ingredient growth factors.[1,35-37] Because these fibroblasts interfere with single-cell live-imaging approaches, we attempted to develop a feeder-free organoid culture system that allows various lung epithelial stem cells to proliferate.

To collect various mouse lung epithelial stem cells, we took advantage of a transgenic reporter mouse line, *SFTPC-GFP*, in which the level of GFP expression varies according to the airway region.[35] EpCAM⁺ lung epithelial cells were collected from *SFTPC-GFP* mice by fluorescence-activated cell sorting (FACS) and divided into three fractions according to the GFP intensity (Supplementary Fig. S1A). Using quantitative reverse transcription polymerase chain reaction (qRT-PCR), we confirmed that the GFP-negative subset (GFPneg) included bronchial airway epithelial cells, such as *Krt5⁺* basal, *Scgb1a1⁺* club, and *Foxj1⁺* ciliated cells. In contrast, the GFP-low subset (GFPlow) had a bronchiolar club and fewer ciliated cells. The GFP-high subset (GFPhi) mainly contained Sftpc⁺ AT2 cells, as previously reported (Supplementary Fig. S1B).[35]

To develop a feeder-free lung organoid culture medium, we optimized growth factor cocktails that are sufficient enough to maintain and induce proliferation of the lung epithelial stem cells. We cultured mouse lung epithelial cells by adding KGF, FGF10, HGF, and inhibitors of TGFβ and BMP signaling (SB431542, NOGGIN) and successfully generated organoids from each GFPhi, GFPlow, and GFPneg population (Fig. 1B; Supplementary Fig. S1C–S1E). Unlike a previous report,[38] the addition of a Wnt agonist, CHIR99021, did not improve the organoid-forming efficiency (OFE) of any subset of lung stem cells (Supplementary Fig. S1F). Our culture system also revealed that the GFPlow cells have better OFE than GFPneg and GFPhi (10% compared to 3%-5%) (Fig. 1C).

To determine the cellular contents of these organoids, we evaluated the mouse lung epithelial cell lineage markers by qRT-PCR and immunocytochemistry at culture day 9 (Fig. 1D–G). As suggested by a previous report,[35] GFPneg organoids expressed bronchial airway epithelial markers, whereas GFPhi organoids showed high expression of the alveolar markers. GFPlow organoids contained club, AT1, and AT2 cells in a sphere that exhibited a mixed phenotype of conducting airway and alveoli (Fig. 1D and 1F). These organoids were further incubated with a basic medium for accelerating differentiation and were examined on day 12 (Fig. 1H). Each GFPneg and GFPhi organoids still showed exclusive expression of bronchial airway epithelial and alveolar markers, respectively (Fig. 1I, 1K, 1L, and 1N). In contrast, GFPlow organoids increased AT1 cell markers, AGER and HOPX, suggesting the progression of alveolar differentiation (Fig. 1J and 1M). Supporting this result, it has been reported that some club cell subpopulations, such as BASCs, UPK3A⁺, and H2-K1⁺, can migrate to the alveolar and transdifferentiate into AT1 and AT2 cells.[22-25,39] These data sets prompted us to hypothesize that club cells in the GFPlow subset include a stem cell subpopulation that forms organoids more efficiently than the other club or AT2 cells and can differentiate into AT1 and AT2 cells in our feeder-free culture condition.

To validate that a part of club cells provides the source of alveolar organoids, we employed *Scgb1a1-CreER*, *Rosa26-mTmG* mice, and the conducting airway epithelial marker CD24 to isolate club cells (Scgb1a1⁺, CD24mid) by separating them from ciliated (Scgb1a1⁺, CD24hi) and AT2 cells (Scgb1a1⁺, CD24neg) using FACS (Fig. 1O). Like the GFPlow organoids, the Scgb1a1⁺, CD24mid cells generated organoids and showed the bronchoalveolar phenotype by day 9 and then further differentiated into alveolar AT1 and AT2 cells by day 12 (Fig. 1P–1S). To ask whether the contaminated AT2 cells expanded in the culture, we excluded AT2 cells by FACS with anti-MHCII antibody. Scgb1a1+, CD24mid, MHCIIneg cells showed similar OFE and differentiation capacity with Scgb1a1+, CD24mid cells, indicating that the influence from contaminated AT2 cells is negligible (Fig. S1H–S1K). These data proved our idea that club cells or their subpopulation can transdifferentiate into alveolar cells with better OFE than AT2 cells.

### Single-Cell Morphometry Following Long-Term Live-Organoid Imaging Unveiled the Morphological Features of the Club-Cell Subpopulation

Studies have demonstrated that particular subpopulations but not all club cells contribute to alveolar tissue regeneration.[21-25] To identify the subpopulation of club cells that can form organoids, we took advantage of long-term live-organoid imaging and retrospective analyses (Fig. 1A, left). For long-term live imaging, the feeder-free culture system was optimized by reducing the concentration of Matrigel from 50% to 2.5% to culture stem cells on the surface of plate (see Methods). Using this optimized method, mouse Scgb1a1⁺, CD24mid club cells were cultured into a microscope equipped with an incubator. They were imaged for 10 days (see Methods), allowing us to examine the entire process of organoid formation from single cells to spheres (Fig. 2A). Reflecting the OFE (12%), only a few cells became organoids, and the others remained as single-cell colonies or formed tiny aggregates (Fig. 2B, red and white arrowheads). To predict subpopulations of club cells on day 0 and determine whether they efficiently form organoids
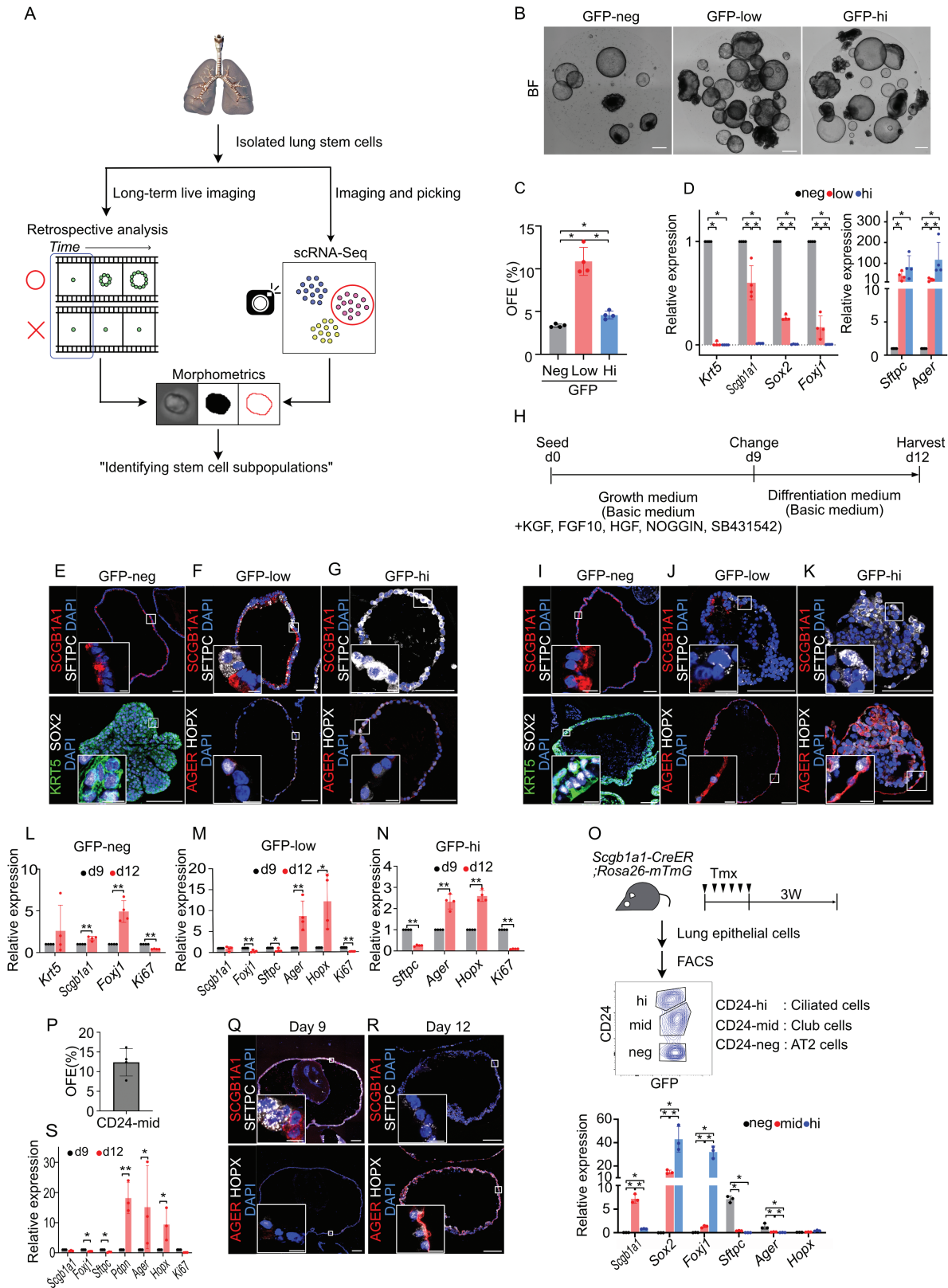
**Figure 1.** Club-cell subpopulation transdifferentiates into alveolar cells. See also Supplementary Fig. S1. (**A**) Overview of the scMORN method. (**B**) Representative bright-field images of organoids at culture day 9. (**C**) OFE of each GFP[neg/low/hi] cells under the feeder-free culture condition (*n* = 3 mice). (**D**) Quantification for lung cell lineage marker expression of day 9 organoids derived from GFP[neg/low/hi] cells. Data are presented as relative expression to GFP[neg] (*n* = 4 mice). Conducting airway genes: *Krt5*, *Scgb1a1*, *Sox2*, and *Foxj1*. Alveolar genes: *Sftpc* and *Ager*. (**E-G**) (**I-K**) Immunostaining of organoids derived from GFP[neg/low/hi] cells for SCGB1A1, SFTPC, KRT5, ACTUB, SOX2, AGER, and HOPX, and DAPI staining at day 9 (E-G) and day 12 (I-K). (**H**) Experimental scheme for lung stem cell amplification culture and differentiation. (**L-N**) Quantification for lung cell lineage marker expression of organoids at days 9 and 12 by qRT-PCR (*n* = 4 mice). Data are presented as the relative expression of each sample at day 9. (**O**) Experimental scheme of sorting Scgb1a1-lineage-positive cells from *Scgb1a1-creER; Rosa26-mTmG* mice. Quantification of lung cell lineage marker expression in the sorted

and provide alveolar cells in the culture system, we attempted to correlate the OFE with the morphological characteristics of individual club cells by analyzing single-cell morphometry. The organoid-forming or non-forming were determined on day 0 by retrospective analysis of organoid-formation assay time-series images (Fig. 2B). One thousand fifty-six single-cell images were collected and classified into organoid-forming (235 images) and non-organoid-forming cells (821 images; Fig. 2C). We quantitatively profiled these 1056 cells in 31 different measurements using ImageJ (Fig. 2D). We found 11 measurements that can statistically distinguish between organoid-forming cells from non-organoid-forming cells (Supplementary Table S1; and see Methods). Most of these measurements are related to cell sizes such as area, length in major axis, and perimeters (Fig. 2E). Of note, the organoid-forming club cells are slightly but significantly large (organoid-forming club cells; 134 $\mu m^2$ ± 37 vs. non-forming club cells; 100 $\mu m^2$ ± 34 (mean ± SD), $P$ = 2.2E−16). Thus, our single-cell morphometric analysis following long-term live-organoid imaging suggests that average-size of the organoid-forming club cells may be larger in comparison to non-organoid-forming cells.

Next, we examined whether isolated solitary large club cells show better organoid-forming capacity than the other club cells. As FACS sorting could not separate those 2 populations due to subtle differences in cell size, we took advantage of an automation system by which individual cells can be imaged, picked up, and transferred to another culture plate (Fig. 2F; Supplementary Movie S1; and Methods). First, isolated mouse Scgb1a1+, CD24mid cells were arrayed on the bottom of an Elplasia microsquare bottom plate. Then, each single cell was imaged with an upright camera, picked by the robot (Fig. 2G), and inoculated into each well of a 384-well plate to culture for organoid assay. The organoid formation was assessed on day 10, and similar to the above experiment, single-cell morphometry analysis using ImageJ was performed on each organoid-forming and nonforming club cells (Fig. 2H), determining that organoid-forming club cells are slightly but statistically larger than nonforming club cells, even in an isolated condition (Fig. 2I). We evaluated the correlation between OFE and cell size distribution and found that club cells showed better OFE as cell size increased (Fig. 2J). These experiments determined a positive correlation between these OFEs and cell size ($R$ = 0.781, $P$ = .000587). If the cell size was more than 150 $\mu m^2$, OFE was approximately 50%. Thus, the large club cells indeed show a better survival rate and high proliferation capacity.

## scRNA-seq Revealed Transcriptional Features of the Club-Cell Subpopulations

These results prompted us to hypothesize that club cells are composed of subpopulations with different organoid-forming capacities, and especially large club cells have a better capacity. Next, we sought mouse club cell subpopulations with different cell sizes to test these ideas. To unveil transcriptional signatures of club cell subpopulations, we performed scRNA-seq analysis following single-cell morphometry. The Scgb1a1+, CD24mid cells were imaged and sorted into PCR plates by cell imaging and picking robot, respectively, and were then analyzed by a plate-based scRNA-seq method (Fig. 1A (right) and 3A). We analyzed 286 cells and found that these cells were divided into 3 distinct groups, club #1, club #2, and AT2, based on gene expression patterns (Fig. 3B and 3C). *Scgb1a1* was dominantly expressed in clubs #1 and #2, while *Sftpc* was expressed only in AT2 (Fig. 3D and 3E). We linked each single-cell expression data to the results of morphometry analysis of the same individual cells. We determined that club #2 was significantly larger than club #1, #1 vs. #2 = 117 ± 25 $\mu m^2$ vs. 125 ± 27 $\mu m^2$ (mean ± SD, $P$ = .02196) (Fig. 3F). This observation suggested that mouse club cell subpopulations are distinguished by unique transcriptomes and different cell size. In club #2, we found 184 genes significantly and more highly expressed than in club#1 (Supplementary Table S2). Because several upregulated genes are relative to the mucus layer and secretory proteins, including *Muc5b*, *Tff2*, *Reg3g*, *Bpifb1,* and *Scgb3a1*, we speculated that club #2 cells appear to be largely due to the large amount of accumulated secretions. We conducted immunocytochemistry and confirmed that SCGB3A1+ club cells were larger than SCGB3A1− club cells (Supplementary Fig. S2A and S2B). Because of its gene expression and cell morphological features, club #2 was named ML (Muc5b+, large)-club cells.

To isolate a large number of ML-club cells, we sought cell surface antigens specific to ML-club cells and found nine distinct antigens (Fig. 3G). We tried to isolate ML-club cells with commercially available antibodies using FACS. Anti-KCNE3 and anti-IL13RA1 antibodies did not work for FACS sorting method; however, anti-CD14 antibody fortunately worked and distinguished CD14-positive and negative (CD14+ and CD14−) with isotype control antibody (Fig. 3H). CD14+ club cells could be isolated from Scgb1a1+, CD24mid cells except for MHCII+ AT2 cells. The expression of *Muc5b, Scgb3a1,* and *Tff2* in CD14+ club cells was confirmed by qRT-PCR (Fig. 3I). Single-cell morphometry further confirmed that CD14+ cells are statistically larger in comparison to CD14− cells (CD14+ vs. CD14− = 107 ± 22 $\mu m^2$ vs. 85 ± 25 $\mu m^2$, Mean ± SD, $P$ = 2.2e−16), suggesting that the CD14 antibody is useful to enrich ML-club cells from Scgb1a1+, CD24mid cells by FACS (Fig. 3J). The CD14+ club cells indeed showed better OFE than CD14− and generated alveolar organoids (CD14+ vs. CD14− = 13.4 ± 2.6% vs. 4.5 ± 1.2%, mean ± SD, $P$ = .0008), which consist of AT1 and AT2 cells by day 12 in the feeder-free organoid culture system (Fig. 3K–3M). In addition, CD14+ cells were assessed for correlation between OFE and cell size. Likewise Scgb1a1+, CD24mid cells (Fig. 3N), and CD14+ cells showed a positive correlation ($R$ = 0.673, $P$ = .00602). These large CD14+ cell-derived (more than 140 $\mu m^2$) organoids expressed all alveolar cells markers (SFTPC, AGER, and HOPX), ML-club cells markers (MUC5B and SCGB3A1), and pan-club cell marker (SCGB1A1) in one organoid at day
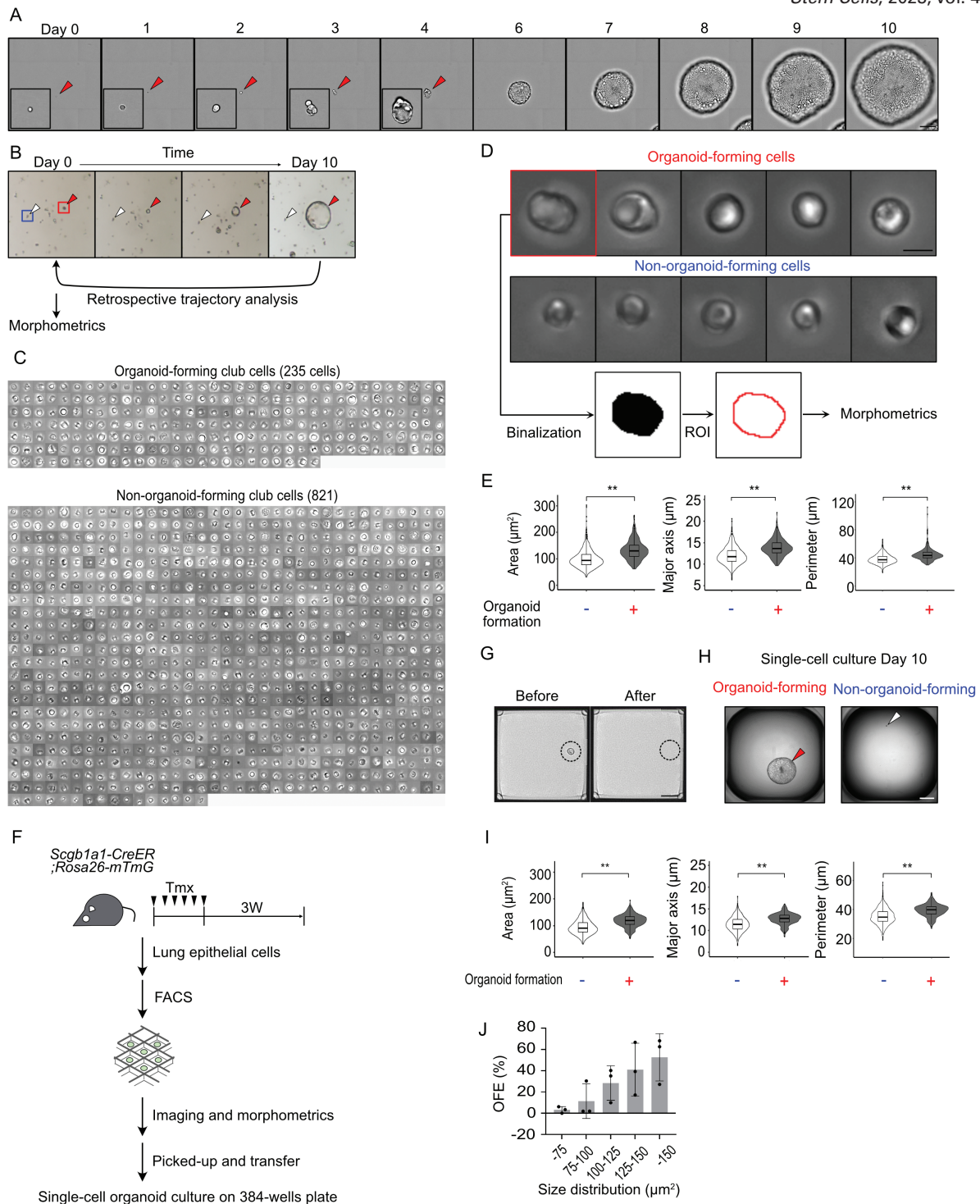
**Figure 2.** Single-cell morphometry following long-term live-organoid imaging unveiled morphological features of the club-cell subpopulation. (**A**) Long-term time-lapse images of developing lung organoid for 10 days. Insets are high magnification images of arrowhead-indicated single cells and organoids. Scale bars: 200 μm. (**B**) Representative images of retrospective trajectory analysis. A stem cell that forms a lung organoid (red arrowheads) and does not form an organoid (white arrowheads) are indicated. (**C**) Each single-cell images of organoid-forming cells (left, *n* = 235) and non-organoid-forming cells (right, *n* = 821) taken by Celldiscoverer7 (see Methods). Scale bars: 10 μm. (**D**) Images of organoid-forming cells (upper) and non-organoid-forming cells (middle) taken by a microscope equipped with an incubator (see Methods). The ImageJ analyzed each single-cell image and lined by ROI. for morphometrics (lower, see Methods for details). Scale bars: 10 μm. (**E**) Violin and box plots of the cell area, the length of the major axis, and perimeter of each single cells (non-organoid-forming cells [*n* = 821], organoid-forming cells [*n* = 235]). These experiments were independently performed 3 times. **$P < .01$ (Wilcoxon rank-sum test). (**F**) Experimental scheme of a series of experiments with single-cell imaging, picking, and organoid culture. (**G**) Representative single-cell image in micro-well of Elplasia. Dashed line circles show the same region before and after picking. Scale bars: 50 μm. (**H**) Organoid culture in 384-well plate at day 10. The red arrowhead indicates growing lung organoid, and the white arrowhead indicates non-organoid-forming cells. Scale bars: 500 μm. (**I**) Violin and box plots of the cell area, the length of major axis and perimeter of each single cell (non-organoid-forming cells [*n* = 746], organoid-forming cells [*n* = 307]). These experiments were independently performed 3 times. **$P < .01$ (Wilcoxon rank-sum test). (**J**) The ratio of organoid forming cells of isolated Scgb1a1+, CD24$^{mid}$ cells at different cell sizes.
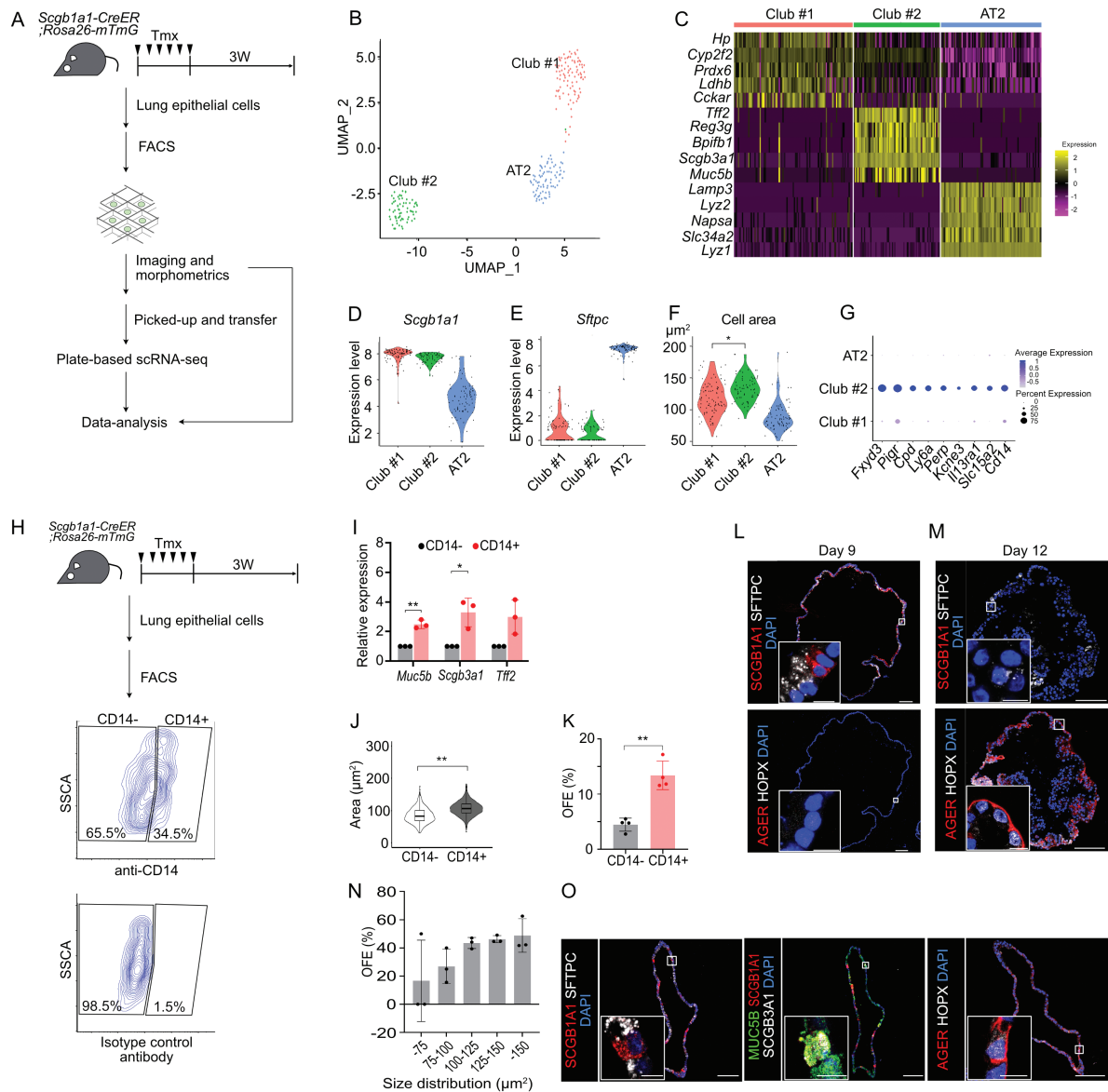
**Figure 3.** scRNA-seq revealed unique transcriptional features of ML-club cells. (**A**) Experimental scheme of a series of experiments with single-cell imaging, picking, and a plate-based scRNA-seq analysis. (**B**) Unsupervised UMAP clustering analysis revealed 3 distinct clusters in Scgb1a1+ and CD24$^{mid}$ cells. (**C**) Heatmap analysis of the 5 top-upregulated genes of each cluster. (**D-F**) Violin plots of expression level of *Scgb1a1* (D), *Sftpc* (E), and cell area distribution (F) of each cluster. *$P < .05$ (Wilcoxon rank-sum test between club #1 and club #2). (**G**) Dot plot analysis of 9 cell surface antigens for club #2. (**H**) Experimental scheme of sorting CD14+ and CD14− club cells using FACS. (**I**) Quantification for ML-club cell marker expression of sorted CD14+ and CD14− club cells by qRT-PCR. Data are presented as relative expression to CD14− club cells and as mean ± SD ($n = 3$ mice). **$P < .01$, *$P < .05$ (2-tailed unpaired Student's $t$-test). (**J**) Violin and box plot of the cell area of each CD14+ ($n = 1353$) and CD14− ($n = 830$) club cells. These experiments were repeated 3 times. **$P < 0.01$ (Wilcoxon rank-sum test). (**K**) OFE of each CD14+ and CD14− club cells. Data are presented as mean ± SD ($n = 4$ mice). **$P < 0.01$ (2-tailed unpaired Student's $t$-test). (**L-M**) Immunostaining of organoids derived from CD14+ club cells for lung cell lineage markers, SCGB1A1, SFTPC, AGER, and HOPX, and DAPI staining at culture day 9 (L) and day 12 (M). (**N**) The ratio of organoid forming cells of isolated CD14+ cells at different cell size ($n = 967$). These experiments were independently performed 3 times. (**O**) Immunostaining of organoids derived from more than 140 μm$^2$ CD14+ club cells for lung cell lineage markers, SCGB1A1, SFTPC, MUC5B, SCGB3A1, AGER, and HOPX, and DAPI staining at culture day 10 with serial sections. Scale bars in images (L, M, O), 100 μm; in enlarged images of the white boxed region, 10 μm (L, M, O).

10 (Fig. 3O). Conclusively, we identified 2 mouse club-cell subpopulations that exhibit different properties in organoid-forming capacity and cell size, and gene expression profile. In particular, we discovered ML-club cells showing high OFE that can be isolated using the cell surface antigen CD14. However, H2-K1+ progenitors also express *Cd14* gene. We will describe this point in the next section.

Through a series of experiments, we established a method for identifying a stem cell subpopulation that has the potential to efficiently form organoids and generate the cell populations we need by combining quantitative data from single-cell morphometrics, organoid-forming assay, and single-cell RNA transcriptome analysis. As a result, this new method was named scMORN.

## Unique Features of ML-Club Cells in Localization and Transcriptome

Previously reported club-cell subpopulations have been shown to exhibit unique localizations on the conducting airways: BASCs on the bronchoalveolar duct junction, UPK3A+ cells around

the neuroepithelial bodies, and H2-K1 progenitors in distal bronchioles.[22-25] To evaluate the localization of ML-club cells on the airway of adult mouse, we performed immunostaining for the pan-club cells and ML-club cell markers (Fig. 4A; Supplementary S2C). While the pan-club cell marker SCGB1A1 detected all club cells throughout the airway epithelium, the ML-club cell markers TFF2, MUC5B, and SCGB3A1 mainly appeared at the main bronchi of the intrapulmonary region (Fig. 4A1–4A2; Supplementary S2C1-S2C2). Most SCGB1A1+ club cells at the main bronchus expressed these 3 ML-club cell markers. In contrast, club cells at the distal bronchiole and bronchoalveolar duct junction did not express these ML-club cell markers, suggesting that ML-club cells are different from known club-cell subpopulations, such as BASCs, UPK3A+, and H2-K1+ cells. We conducted immunohistochemistry for secreted proteins (SCGB1A1, SCGB3A1, and MUC5B) and observed that the proximal club cells accumulated these secreted proteins into vesicle-like structures, supporting the idea that ML-club cells appear to be largely due to the large amount of accumulated secretions (Fig. 4B and 4C).

To confirm the unique genetic features of ML-club cells, we combined our data and previously published single-cell transcriptome data of BASCs[24] and analyzed them (Fig. 4D). ML-club cells showed a distinct cluster from the 2 BASCs that include BASCs#1 and BASCs#2 expressing specific markers, *Mfsd2a* and *Lamb3*, respectively; AT2 cells, which express *Sftpc*; and ciliated cells, which express *Foxj1* (Fig. 4E; Supplementary S2D). BASCs and ciliated cells express lower levels of *Scgb1a1* than pan-club cells including ML-club cells. In the ML-club cell cluster, neither *H2-K1* nor *Upk3a* was accumulated, whereas high *Muc5b* and *Scgb3a1* expression were detected (Supplementary Fig. S2D), demonstrating that ML-club cells have a distinct transcriptional feature from BASCs, UPK3A+, and H2-K1+ cells at least in in silico analysis. On the contrary, H2-K1+ cells express *Cd14*,[22] making it difficult to completely separate ML-club cells from H2-K1+ cells by FACS. To overcome this issue, the proximal and distal conducting airways were surgically separated and CD14+ club cells were isolated from each tissue (Fig. 4F). Proximal CD14+ cells accumulated ML-club cells confirmed by qPCR (Fig. 4G). Interestingly, the OFE of the proximal CD14+ cells were higher than that of distal CD14+ cells (Fig. 4H). We further confirmed that proximal and distal CD14+ cells can differentiate into alveolar epithelial cells in differentiation medium by qPCR and IHC (Fig. 4I–4N). The proximal and distal CD14+ cells differentiated into alveolar cells but the proximal CD14+ cell-derived organoids tended to express ML-club cell markers. Unexpectedly, these ML-club cell-derived organoids are positive for p63 but not Krt5 and basal cell markers (Supplementary Fig. S2E and S2F). This observation might reflect transitional state between conducting airway and alveolar epithelial states (see Discussion). These results demonstrate that ML-club cells are distinct from other club-cell subpopulations and have relatively high viability.

Based on these results, we propose that ML-club cells are a new club-cell subpopulation that can generate alveolar epithelial cells in vitro and shows better OFE than other club and AT2 cells, at least in our organoid culture system.

### ML-club Cells are Engrafted and Expanded In Vivo More Efficiently Than Other Club and AT2 Cells

To determine the stem cell capacity of ML-club cells in vivo, we performed a transplantation assay with the proximal CD14+ club cells enriched for ML-club cells. We prepared 3400 GFP-expressing CD14+ cells from the proximal airways which is the maximum number of cells that can be collected from one transgenic mouse, 7000 GFP-expressing CD14+ and CD14- club cells from whole lungs of *Scgb1a1-CreER; Rosa26-mTmG* mouse lines, and Sftpc+ AT2 cells from *Sftpc-creERT2*; and *Rosa26-mTmG* mouse lines to transplant into nude mice. Three mice in each group were injured by bleomycin inhalation to model an acute lung injury (Fig. 5A). If ML-club cells have a better proliferation capacity than other lung epithelial stem cells, the proximal CD14+ cells should expand more at the engrafted region than other types of lung epitheliums (CD14+, CD14-, and AT2 cells). Two weeks after transplantation, the GFP of transplanted lungs indicated engrafted cells at the injured region. GFP+ cells appeared to form foci, reflecting a clonal expansion of engrafted cells. As we expected, the proximal CD14+ cells formed larger foci than CD14- or AT2 cells (Fig. 5B; Supplementary S3). We quantified the number of cells within a focus and found that the proximal CD14+ foci contain significantly more cells than others, reflecting the better proliferation capacity, while there is no significant difference in cluster formation efficiency (Fig. 5C and 5D). We further performed immunostainings for alveolar cell types to evaluate the alveolar differentiation of engrafted cells. PDPN and SFTPC were detected in the proximal CD14+ cells-derived GFP+ clusters (Fig. 5E). Most of the transplanted cells were differentiated into SFTPC+ alveolar or SCGB1A1+ bronchiolar cells, whereas the minor SFTPC+, SCGB1A1+, double-positive cells, and unstained cells were also observed (Fig. 5F and 5G).

## Discussion

Investigating the heterogeneity of adult tissue stem cells is still challenging because these cells are often in a dormant state, and single-cell RNA sequencing does not directly link the stem cells' potential to their expression profiles. Here, we established the scMORN method, a new single-cell analysis method, for profiling the organoid-forming capacity of tissue stem cells by integrating single-cell morphometrics, organoid-forming assay, and single-cell RNA sequencing.

In this study, single-cell morphometry and long-term live-organoid imaging of isolated club cells were used to examine the relations between stem cell morphological features and organoid-formation potential. A morphological feature of organoid-forming club cells, especially the cell size, was found in a retrospective analysis. These club cells are relatively larger than other club cells on average and can differentiate into alveolar cells. We further revealed the single-cell transcriptome of the club cells by combining automated single-cell picking technology with scRNA-seq. Based on the genetic characteristics and morphometric features of this subpopulation, we named it "ML-club cells." An in vivo transplantation experiment with the injured lung confirmed that the proximal CD14+ club cells, which enrich ML-club cells, engraft and expand at the damaged area more efficiently than CD14- club cells or AT2 cells and differentiate into alveolar cells that are consistent with the situation in in vitro organoid culture. Higher engraftment efficiency of ML-club cells than AT2 cells, consistent with a recent study, shows the need for the higher number of mature AT2 cells for effective engraftment.[22,40] Although, our accumulation method using anti-CD14 antibody is not effective enough to purify ML-club cells due to
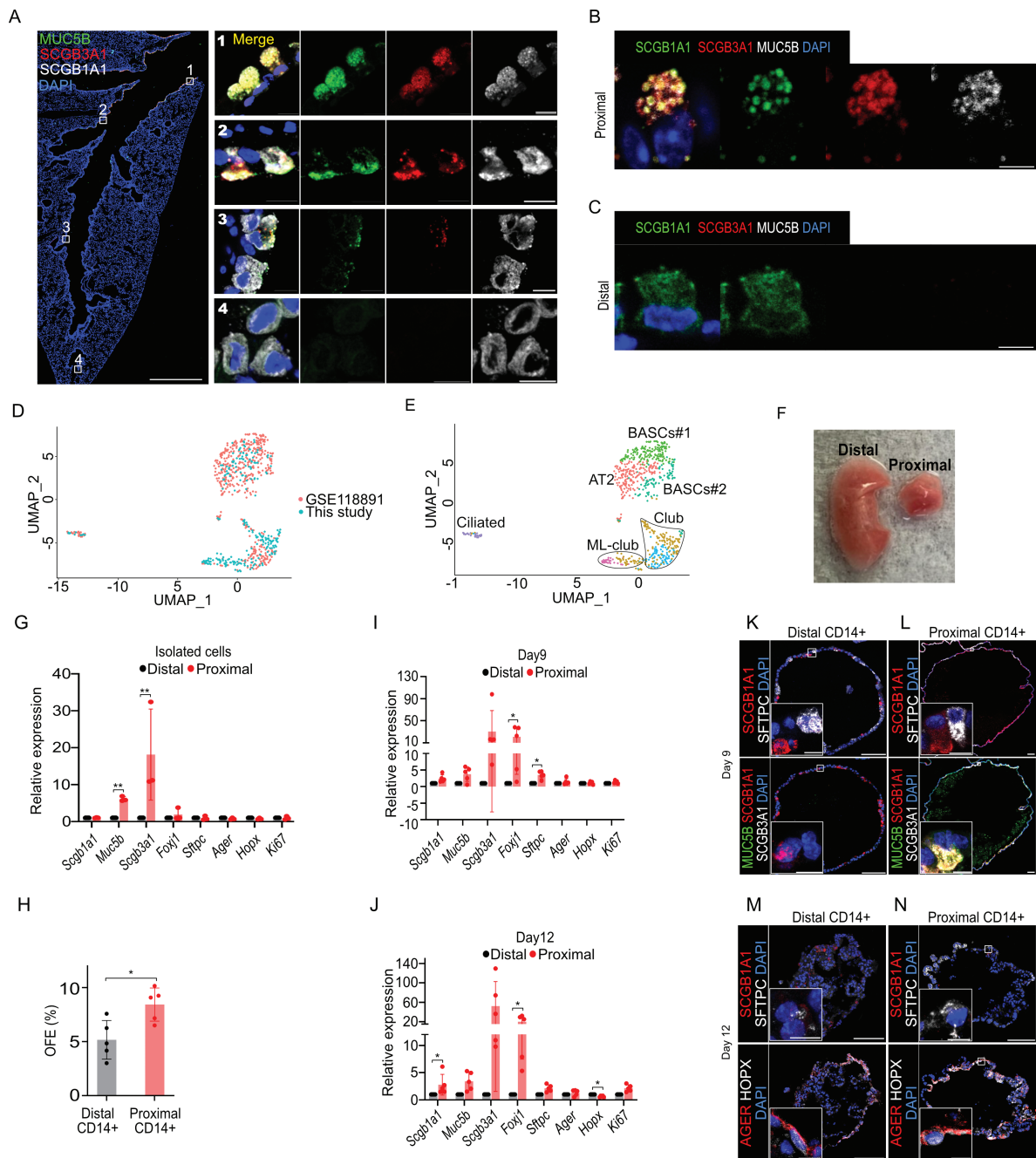
**Figure 4.** Unique features of ML-club cells in localization and transcriptome. See also Supplementary Fig. S2. (**A**) Distribution of club and ML-club cells in adult lung detected by immunostaining for MUC5B, SCGB3A1, and SCGB1A1, and DAPI staining. Scale bars in the left panel, 1 mm; in enlarged images, 10 μm. (**B and C**) Representative proximal (B) and distal (C) airway cell image immunostained for SCGB1A1, SCGB3A1, and MUC5B. Scale bars in images, 5 μm. (**D and E**) Dimension plot (D) and unsupervised UMAP clustering analysis (E) of integrated data of GSE118891 and this study's data. (**F**) Image of distal and proximal region of left lobe. (**G**) qPCR analysis was performed using isolated distal and proximal CD14+ club cells. Data are presented as relative expression of distal CD14+ cells. (**H**) OFE of each distal and proximal CD14+ club cells (*n* = 5 mice). (**I and J**) qPCR analysis was performed using organoids derived from distal and proximal CD14+ Scgb1a1-lineage cells at day9 (I) and day12 (J) (*n* = 5 mice). Data are presented as relative expression of distal CD14+ organoids. All quantification data are presented as mean ± SD **P < .01, *P < .05 using two-tailed unpaired Student's *t*-test (G, H, I, J). (**K-N**) Immunostaining of organoids derived from distal and proximal CD14+ club cells for lung cell lineage markers, SCGB1A1, SFTPC, MUC5B, SCGB3A1, AGER, and HOPX, and DAPI staining at culture day 9 (K and L) and day 12 (M and N). Scale bars in images, 100 μm; in enlarged images of the white boxed region, 10 μm.

contamination of several small-club cells (Fig. 3J and 3K). The genetic labeling approach for ML-club cells using Muc5b-CreER or Scgb3a1-CreER would overcome this issue in future study. In our organoid culture, organoids generated from the proximal and distal CD14+ cells coexpressed P63 and SFTPC not KRT5 at day 9 (Supplementary Fig. S2E–S2H).

The functions of p63 in alveolar regeneration were reported and were under discussion.[41,42] Our finding might indicate that p63 expression in airway epithelial cells reflects the intermediated state of transdifferentiation into alveolar epithelial cells. In humans, *MUC5B* upregulation caused by the single-nucleotide polymorphism on the promoter region is
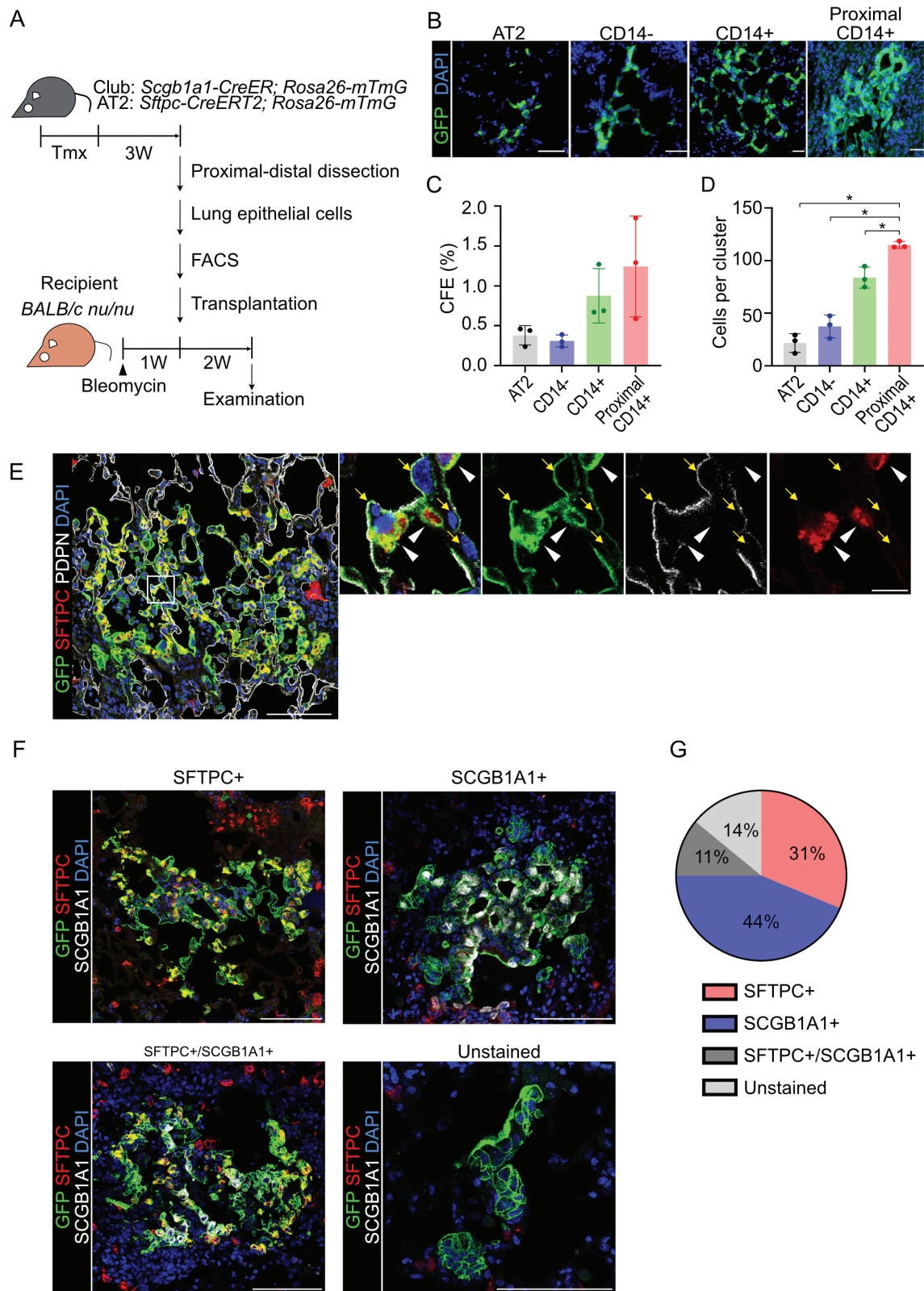
**Figure 5.** ML-club cells are engrafted and expand in vivo more than other club and AT2 cells. See also Supplementary Fig. S3. (**A**) Experimental scheme of club and AT2 cells transplantation into bleomycin-injured nude mice. (**B**) Detection of transplanted AT2, CD14− club, CD14+ club, and proximal CD14+ club cells with GFP fluorescence. Scale bars: 50 μm. (**C-D**) Quantification of the CFE (cluster formation efficiency) (C) and the number of GFP+ cells per cluster (D) in the lungs transplanted with AT2, CD14−, CD14+, and proximal CD14+ club cells. Data are presented as mean ± SD (*n* = 3 mice). *$P < .05$ (one-way ANOVA followed by Tukey's multiple comparisons test). (**E**) Immunostaining to detect transplanted GFP-expressing proximal CD14+ club and lung lineage markers, Sftpc and Pdpn, and DAPI staining. Right panels show higher magnification of the white boxed region. Arrowheads for Sftpc-expressing GFP+ cells. Arrows for PDPN-expressing GFP+ cells. Scale bars in the left panel, 50 μm; in enlarged images, 10 μm. (**F**) Immunostaining to determine colocalization of GFP and lung lineage markers, SFTPC and SCGB1A1. Scale bars: 50 μm. (**G**) The pie chart shows the ratio of lineage-positive GFP clusters (*n* = 128 clusters from 3 different experiments).

associated with familial interstitial pneumonia and idiopathic pulmonary fibrosis.[43] Hence, in the future, we should investigate this population more to know whether ML-club cells contribute to proper tissue regeneration or pathological disorder in pulmonary disease.

The scMORN method could be improved by overcoming some technical limitations. We performed live imaging and single-cell picking as different procedures because a machine equipped with both options does not exist. Future improvements in machines would shorten the experimental procedures and achieve high-resolution imaging to distinguish subtle morphological features by machine learning.

It has been attempted to predict cellular states from cell morphology by quantifying single-cell morphological information and connecting it with scRNA-seq data. For example, single-cell imaging and scRNA-seq of fission yeast revealed that gene expression patterns were tightly related to cell size.[44] Integrating analysis with human glioblastoma samples also unveiled that there is a clear correlation between the major gene expression and basic imaging features for the malignantly transformed cells in this tumor.[45] Our study successfully identified the lung stem cell subpopulation using the scMORN method. Because human lung cells are able to expand in our feeder-free organoid culture system, the scMORN method would be applied to study human lung cells to find therapeutic resources (Supplementary Fig. S1G). Thus, such meta-analysis combining single-cell morphometry, functional assay, and scRNA-seq analysis has a lot of potential for further improvement of stem cell science and medical applications.

## Conclusion

We established in vitro scMORN method to identify cells with stem cell potential. With this method, we identified a subpopulation of club cells called ML-club cells that show a high capacity for proliferation and differentiation into bronchoalveolar cells in both in vitro organoid culture and in vivo transplantation experiments. This method has potential for application to human lung cells and other types of tissue cells.

## Acknowledgments

## Funding

## Conflict of Interest

## Author Contributions

## Data Availability

All sequencing data are available from the NCBI Sequence Read Archive under accession GSE189917. All image data will be available from SSBD:database [https://ssbd.riken.jp/database/].

## Supplementary material

Supplementary material is available at *Stem Cells* online.

## References

1. Barkauskas CE, Cronce MJ, Rackley CR, et al. Type 2 alveolar cells are stem cells in adult lung. *J Clin Invest*. 2013;123(7):3025-3036. https://doi.org/10.1172/JCI68782.

2. Barker N, Huch M, Kujala P, et al. Lgr5(+ve) stem cells drive self-renewal in the stomach and build long-lived gastric units in vitro. *Cell Stem Cell*. 2010;6(1):25-36. https://doi.org/10.1016/j.stem.2009.11.013.

3. Fatehullah A, Tan SH, Barker N. Organoids as an in vitro model of human development and disease. *Nat Cell Biol*. 2016;18(3):246-254. https://doi.org/10.1038/ncb3312.

4. Huch M, Dorrell C, Boj SF, et al. In vitro expansion of single Lgr5+ liver stem cells induced by Wnt-driven regeneration. *Nature*. 2013;494(7436):247-250. https://doi.org/10.1038/nature11826.

5. Karthaus WR, Iaquinta PJ, Drost J, et al. Identification of multipotent luminal progenitor cells in human prostate organoid cultures. *Cell*. 2014;159(1):163-175. https://doi.org/10.1016/j.cell.2014.08.017.

6. Sato T, Vries RG, Snippert HJ, et al. Single Lgr5 stem cells build crypt-villus structures in vitro without a mesenchymal niche. *Nature*. 2009;459(7244):262-265. https://doi.org/10.1038/nature07935.

7. Chua CW, Shibata M, Lei M, et al. Single luminal epithelial progenitors can generate prostate organoids in culture. *Nat Cell Biol*. 2014;16(10):951-61, 1. https://doi.org/10.1038/ncb3047.

8. DeWard AD, Cramer J, Lagasse E. Cellular heterogeneity in the mouse esophagus implicates the presence of a nonquiescent epithelial stem cell population. *Cell Rep*. 2014;9(2):701-711. https://doi.org/10.1016/j.celrep.2014.09.027.

9. Huch M, Gehart H, van Boxtel R, et al. Long-term culture of genome-stable bipotent stem cells from adult human liver. *Cell*. 2015;160(1-2):299-312. https://doi.org/10.1016/j.cell.2014.11.050.

10. Zepp JA, Zacharias WJ, Frank DB, et al. Distinct mesenchymal lineages and niches promote epithelial self-renewal and myofibrogenesis in the Lung. *Cell*. 2017;170(6):1134-1148.e10. https://doi.org/10.1016/j.cell.2017.07.034.

11. Lukonin I, Serra D, Challet Meylan L, et al. Phenotypic landscape of intestinal organoid regeneration. *Nature*. 2020;586(7828):275-280. https://doi.org/10.1038/s41586-020-2776-9.

12. Hogan BL, Barkauskas CE, Chapman HA, et al. Repair and regeneration of the respiratory system: complexity, plasticity, and mechanisms of lung stem cell function. *Cell Stem Cell*. 2014;15(2):123-138. https://doi.org/10.1016/j.stem.2014.07.012.

13. Kiyokawa H, Morimoto M. Molecular crosstalk in tracheal development and its recurrence in adult tissue regeneration. *Dev Dyn*. 2021;250(11):1552-1567. https://doi.org/10.1002/dvdy.345.

14. Kotton DN, Morrisey EE. Lung regeneration: mechanisms, applications and emerging stem cell populations. *Nat Med*. 2014;20(8):822-832. https://doi.org/10.1038/nm.3642.

15. Adamson IY, Bowden DH. The type 2 cell as progenitor of alveolar epithelial regeneration. A cytodynamic study in mice after exposure to oxygen. *Lab Invest*. 1974;30(1):35-42.

16. Desai TJ, Brownfield DG, Krasnow MA. Alveolar progenitor and stem cells in lung development, renewal and cancer. *Nature*. 2014;507(7491):190-194. https://doi.org/10.1038/nature12930.

17. Rock JR, Hogan BL. Epithelial progenitor cells in lung development, maintenance, repair, and disease. *Annu Rev Cell Dev Biol*. 2011;27:493-512. https://doi.org/10.1146/annurev-cellbio-100109-104040.

18. Nabhan AN, Brownfield DG, Harbury PB, Krasnow MA, Desai TJ. Single-cell Wnt signaling niches maintain stemness of alveolar type 2 cells. *Science*. 2018;359(6380):1118-1123. https://doi.org/10.1126/science.aam6603.

19. Zacharias WJ, Frank DB, Zepp JA, et al. Regeneration of the lung alveolus by an evolutionarily conserved epithelial progenitor. *Nature*. 2018;555(7695):251-255. https://doi.org/10.1038/nature25786.

20. Rock JR, et al. Multiple stromal populations contribute to pulmonary fibrosis without evidence for epithelial to mesenchymal transition. *Proc Natl Acad Sci U S A*. 2011;108:E1475-E1483. https://doi.org/10.1073/pnas.1117988108.

21. Kim CF, Jackson EL, Woolfenden AE, et al. Identification of bronchioalveolar stem cells in normal lung and lung cancer. *Cell*. 2005;121(6):823-835. https://doi.org/10.1016/j.cell.2005.03.032.

22. Kathiriya JJ, Brumwell AN, Jackson JR, Tang X, Chapman HA. Distinct airway epithelial stem cells hide among club cells but mobilize to promote alveolar regeneration. *Cell Stem Cell*. 2020;26(3):346-358.e4. https://doi.org/10.1016/j.stem.2019.12.014.

23. Guha A, Deshpande A, Jain A, Sebastiani P, Cardoso WV. Uroplakin 3a(+) cells are a distinctive population of epithelial progenitors that contribute to airway maintenance and post-injury repair. *Cell Rep*. 2017;19(2):246-254. https://doi.org/10.1016/j.celrep.2017.03.051.

24. Liu Q, Liu K, Cui G, et al. Lung regeneration by multipotent stem cells residing at the bronchioalveolar-duct junction. *Nat Genet*. 2019;51(4):728-738. https://doi.org/10.1038/s41588-019-0346-6.

25. Salwig I, Spitznagel B, Vazquez-Armendariz AI, et al. Bronchioalveolar stem cells are a main source for regeneration of distal lung epithelia in vivo. *EMBO J*. 2019;38(12):e102099. https://doi.org/10.15252/embj.2019102099.

26. Vaughan AE, Brumwell AN, Xi Y, et al. Lineage-negative progenitors mobilize to regenerate lung epithelium after major injury. *Nature*. 2015;517(7536):621-625. https://doi.org/10.1038/nature14112.

27. Hong KU, Reynolds SD, Giangreco A, Hurley CM, Stripp BR. Clara cell secretory protein-expressing cells of the airway neuroepithelial body microenvironment include a label-retaining subset and are critical for epithelial renewal after progenitor cell depletion. *Am J Respir Cell Mol Biol*. 2001;24(6):671-681. https://doi.org/10.1165/ajrcmb.24.6.4498.

28. Sueblinvong V, Weiss DJ. Stem cells and cell therapy approaches in lung biology and diseases. *Transl Res*. 2010;156(3):188-205. https://doi.org/10.1016/j.trsl.2010.06.007.

29. Fan HC, Fu GK, Fodor SP. Expression profiling. Combinatorial labeling of single cells for gene expression cytometry. *Science*. 2015;347(6222):1258367. https://doi.org/10.1126/science.1258367.

30. Klein AM, Mazutis L, Akartuna I, et al. Droplet barcoding for single-cell transcriptomics applied to embryonic stem cells. *Cell*. 2015;161(5):1187-1201. https://doi.org/10.1016/j.cell.2015.04.044.

31. Macosko EZ, Basu A, Satija R, et al. Highly parallel genome-wide expression profiling of individual cells using nanoliter droplets. *Cell*. 2015;161(5):1202-1214. https://doi.org/10.1016/j.cell.2015.05.002.

32. Lo B, Hansen S, Evans K, Heath JK, Wright JR. Alveolar epithelial type II cells induce T cell tolerance to specific antigen. *J Immunol*. 2008;180(2):881-888. https://doi.org/10.4049/jimmunol.180.2.881.

33. Muzumdar MD, Tasic B, Miyamichi K, Li L, Luo L. A global double-fluorescent Cre reporter mouse. *Genesis*. 2007;45(9):593-605. https://doi.org/10.1002/dvg.20335.

34. Rawlins EL, Okubo T, Xue Y, et al. The role of Scgb1a1+ Clara cells in the long-term maintenance and repair of lung airway, but not alveolar, epithelium. *Cell Stem Cell*. 2009;4(6):525-534. https://doi.org/10.1016/j.stem.2009.04.002.

35. Chen H, et al. Airway epithelial progenitors are region specific and show differential responses to bleomycin-induced lung injury. *Stem Cells*. 2012;30:1948-1960. https://doi.org/10.1002/stem.1150.

36. Lee JH, et al. Anatomically and functionally distinct lung mesenchymal populations marked by Lgr5 and Lgr6. *Cell*. 2017;170:1149-1163. https://doi.org/10.1016/j.cell.2017.07.028.

37. McQualter JL, Yuen K, Williams B, Bertoncello I. Evidence of an epithelial stem/progenitor cell hierarchy in the adult mouse lung. *Proc Natl Acad Sci U S A*. 2010;107:1414-1419. https://doi.org/10.1073/pnas.0909207107.

38. Aros CJ, Pantoja CJ, Gomperts BN. Wnt signaling in lung development, regeneration, and disease progression. *Commun Biol*. 2021;4(1):601. https://doi.org/10.1038/s42003-021-02118-w.

39. Choi J, Jang YJ, Dabrowska C, et al. Release of Notch activity coordinated by IL-1β signalling confers differentiation plasticity of airway progenitors via Fosl2 during alveolar regeneration. *Nat Cell Biol*. 2021;23(9):953-966. https://doi.org/10.1038/s41556-021-00742-6.

40. Weiner AI, Jackson SR, Zhao G, et al. Mesenchyme-free expansion and transplantation of adult alveolar progenitor cells: steps toward cell-based regenerative therapies. *NPJ Regen Med*. 2019;4:17. https://doi.org/10.1038/s41536-019-0080-9.

41. Lv Z, et al. Airway secretory cell-derived p63⁺ progenitors contribute to alveolar regeneration after sterile lung injury. *bioRxiv*, 2023.02.27.530122. https://doi.org/10.1101/2023.02.27.530122.

42. Weiner AI, Zhao G, Zayas HM, et al. ΔNp63 drives dysplastic alveolar remodeling and restricts epithelial plasticity upon severe lung injury. *Cell Rep*. 2022;41(11):111805. https://doi.org/10.1016/j.celrep.2022.111805.

43. Seibold MA, Wise AL, Speer MC, et al. A common MUC5B promoter polymorphism and pulmonary fibrosis. *N Engl J Med*. 2011;364(16):1503-1512. https://doi.org/10.1056/NEJMoa1013660.

44. Saint M, Bertaux F, Tang W, et al. Single-cell imaging and RNA sequencing reveal patterns of gene expression heterogeneity during fission yeast growth and adaptation. *Nat Microbiol*. 2019;4(3):480-491. https://doi.org/10.1038/s41564-018-0330-4.

45. Liu Z, Yuan J, Lasorella A, et al. Integrating single-cell RNA-seq and imaging with SCOPE-seq2. *Sci Rep*. 2020;10(1):19482. https://doi.org/10.1038/s41598-020-76599-w.